Chemical Papers (2020) 74:1027–1037
https://doi.org/10.1007/s11696-019-00942-3

ORIGINAL PAPER

A sensitive and selective electrochemical sensor for the simultaneous determination of trace Cd^{2+} and Pb^{2+}

Jinbang Mei[1] · Zhihua Ying[1] · Wei Sheng[1] · Jie Chen[1] · Junming Xu[1] · Peng Zheng[1]

Received: 25 April 2019 / Accepted: 17 September 2019 / Published online: 23 September 2019

Abstract

A neoteric sensor for the detection of Cd^{2+} and Pb^{2+} has been investigated. The sensor was investigated based on a glutathione/gold nanoparticles/amino-reduced graphene oxide (GSH/AuNPs/NH_2-rGO) nanocomposite, which was decorated on a polished glassy carbon electrode. The characterization analysis of the nanocomposite was performed with scanning electron microscopy, electrochemical techniques, and FTIR. The results indicated that GSH/AuNPs/NH_2-rGO/GCE exhibited excellent analytical performance in detecting Cd^{2+} and Pb^{2+} owing to its large surface area, numerous functional groups, and good electrical conductivity. Under optimized experimental conditions, the stripping peak currents were linear with the concentrations of Cd^{2+} and Pb^{2+} in the scope of 1–120 µg/L with the detection limits of 0.09 µg/L for Cd^{2+} and 0.38 µg/L for Pb^{2+} (S/N = 3). Also, the electrochemical sensor displayed excellent selectivity and reproducibility. Hence, this research revealed that GSH/AuNPs/NH_2-rGO nanocomposite was a promising sensing material for the detection of Cd^{2+} and Pb^{2+}.

Keywords Nanocomposites · Simultaneous detection · Heavy metal ions · Sensor

Introduction

Heavy metals have been severe menaces to human life and ecotope due to their low degradation and toxicity, which can greatly harm the body and natural environment. Among them, Cd^{2+} and Pb^{2+} were two typical pollutants generated from the chemical industries and commonly found in soils (Zhao et al. 2016). The potable water that contained a high content of Pb^{2+} would lead to sickness, such as stomachache, tremble, neurological irritability, along with reduced synapses (Guo et al. 2017). Cd^{2+} was also applied in industries, including serving as a sterilizing agent and manufacturing alloy, and its enrichment in the blood caused passive influences such as gingival macula and osteoporosis (Gupta et al. 2013). Over the past few decades, many analytical methods, including surface enhanced Raman spectrometry (SERS) (Ma et al. 2012), atomic absorption spectrometry (AAS) (Bagheri et al. 2012), atomic fluorescence spectrometry (AFS) (Guzmánmar et al. 2011) and atomic emission spectrometry (AES) (Ho et al. 2010), have been applied in heavy metals analysis. However, these methods have some disadvantages, such as bulkiness, expensive apparatuses, and complications in operation, making them unsuitable for in-site analysis.

For nearly 10 years, electrochemical stripping techniques were well known for determining heavy metal ions due to its high sensitivity and anti-interference ability (Cheng et al. 2016; Choi et al. 2015), but the technology of electrochemical detection mainly hinged on the preconcentration of target ions; so, it was crucial to improve the preconcentration effect. Furthermore, the bismuth film gradually replaced mercury film in electrochemical stripping techniques due to its environment-friendly character and ability to form alloys with heavy metals (Injang et al. 2010; Zhao et al. 2016).

Graphene, an interesting two-dimensional nanomaterial, has been widely considered in the area of electrochemical sensors on account of its high electrical conductivity and large surface area (Ruecha et al. 2015). However, pure graphene was insoluble and showed low adsorption capacity to heavy metal ions with its hydrophobic property (Xing et al. 2016). After it was functionalized with amino groups, amino-reduced graphene oxide (NH_2-rGO) was soluble and could adsorb heavy metal ions through complexing action. But the NH_2-rGO sheets tended to agglomerate and even restack because of its strong π–π

✉ Zhihua Ying
yingzh@hdu.edu.cn

[1] College of Electronics and Information, Hangzhou Dianzi University, Hangzhou 310018, People's Republic of China

stacking and Van Der Waals interactions among individual graphene sheets (Huang et al. 2015). To prevent the aggregation of NH_2-rGO, some metals and metal oxides were utilized to improve the dispersibility of graphene (Han et al. 2017; Xie et al. 2015), and gold nanoparticle (AuNP) was an ideal material to master this problem. In addition, AuNPs, with high surface reactivity, good electrical conductivity and strong adsorption property, have been used to develop sensitive electrochemical sensors for different analytes (Wang et al. 2012). Glutathione (GSH) is a tripeptide that is comprised of glutamate, cysteine, and glycine, which contain abundant ligands for a vast variety of metal ions, including amino, nitrogen functional groups, –COOH and –SH. Especially, GSH can be strongly anchored on AuNPs through the bond of S–Au.

In this work, we first reported the fabrication of Bi/GSH/AuNPs/NH_2-rGO nanocomposite and applied it for the sensitive detection of Cd^{2+} and Pb^{2+} by differential pulse anodic stripping voltammetry (DPASV). Under optimal conditions, the decorated electrode demonstrated excellent sensitivity and selectivity for the analysis of target metal ions. Finally, the propositional sensor was exploited for the simultaneous determination of Cd^{2+} and Pb^{2+} in tap water samples with a satisfying result.

Experimental

Chemicals

The NH_2-rGO was purchased from Nanjing XFNANO Nanomaterials Technology Co., Ltd. (Nanjing, China). NaAc and HAc were purchased from Wuxi ZHANWANG Co., Ltd. (Wuxi, China). $HAuCl_4$ was acquired from Sinopharm Chemical Reagent Co., Ltd. (Shanghai, China). Glutathione (GSH) was obtained from Shanghai Macklin Biochemical Co., Ltd. (Shanghai, China). Acetate buffer solutions were obtained by mixing HAc and NaAc solutions. All these solutions were prepared using deionized water and all chemicals were of analytical grade.

Apparatus

The experiments were implemented on a CHI660E electrochemical workstation (Chenhua Instrument, Shanghai, China) and the three-electrode system consisted of a glassy carbon electrode, a KCl-saturated calomel electrode, and a platinum plate. Scanning electron microscopy analysis and EDS were obtained by JEOL 6460 microscope (Japan). The infrared spectral result was tested by Nicolet Nexus iS5 FTIR spectrometer (Nicolet, USA).

Synthesis of NH_2-rGO/AuNPs/GSH

For the fabrication of GSH/AuNPs/NH_2-rGO (Scheme 1a), 2 mg NH_2-rGO was dispersed in 3 mL deionized water through ultrasonication for 60 min. Next, 250 µL 1% $HAuCl_4$ solution was added and the mixture solution was heated to 60 °C. Then 500 µL 0.1 M trisodium citrate was mixed into this solution under stirring for 90 min (Zhu et al. 2014). After the reaction, the obtained AuNPs/NH_2-rGO composite was cleaned by centrifugation with deionized water. Subsequently, the black precipitate was mixed with GSH by stirring for at least 4 h. Finally, the resulting mixture of GSH/AuNPs/NH_2-rGO was obtained through centrifugation.

Pretreatment of the modified GCE

First, a bare GCE was sequentially polished with 1.0, 0.3, 0.05 µm alumina powder. Then, it was cleaned with deionized water, ethanol, and deionized water by ultrasonic. After the electrode was dried in air, 5 µL of the prepared GSH/AuNPs/NH_2-rGO suspension was modified on the cleaned bare GCE surface using a microsyringe. NH_2-rGO/GCE and AuNPs/NH_2-rGO/GCE were acquired by the same method for comparison.

Procedure of the DPASV analysis

As shown in Scheme 1b, the DPASV was implemented in a 25 mL electrolytic cell that contained 20 mL 0.1 M HAc–NaAc buffer solution, 200 µg/L Bi^{3+} and appropriate amounts of target metal ions. The deposition was performed at − 1.4 V for 300 s under stirring conditions. In the meantime, the target metals and Bi^{3+} were deposited on the surface of the working electrode. After the preconcentration process, a stripping process was performed by DPASV in the potential scope of − 1.1 to − 0.1 V under these conditions: potential step of 4 mV; sample width of 0.0167 s; and quiet time of 30 s.

Results and discussion

Characterization of the nanocomposites

As shown in Fig. 1, the surface morphology of NH_2-rGO, AuNPs/NH_2-rGO and GSH/AuNPs/NH_2-rGO was studied by SEM. The NH_2-rGO film showed a wrinkled and compact structure (Fig. 1a). Compared with NH_2-rGO, the AuNPs/NH_2-rGO composite was composed of an ultrathin sheet decorated with dispersive AuNPs (Fig. 1b), which can serve as spacers to prevent the agglomeration of NH_2-rGO.

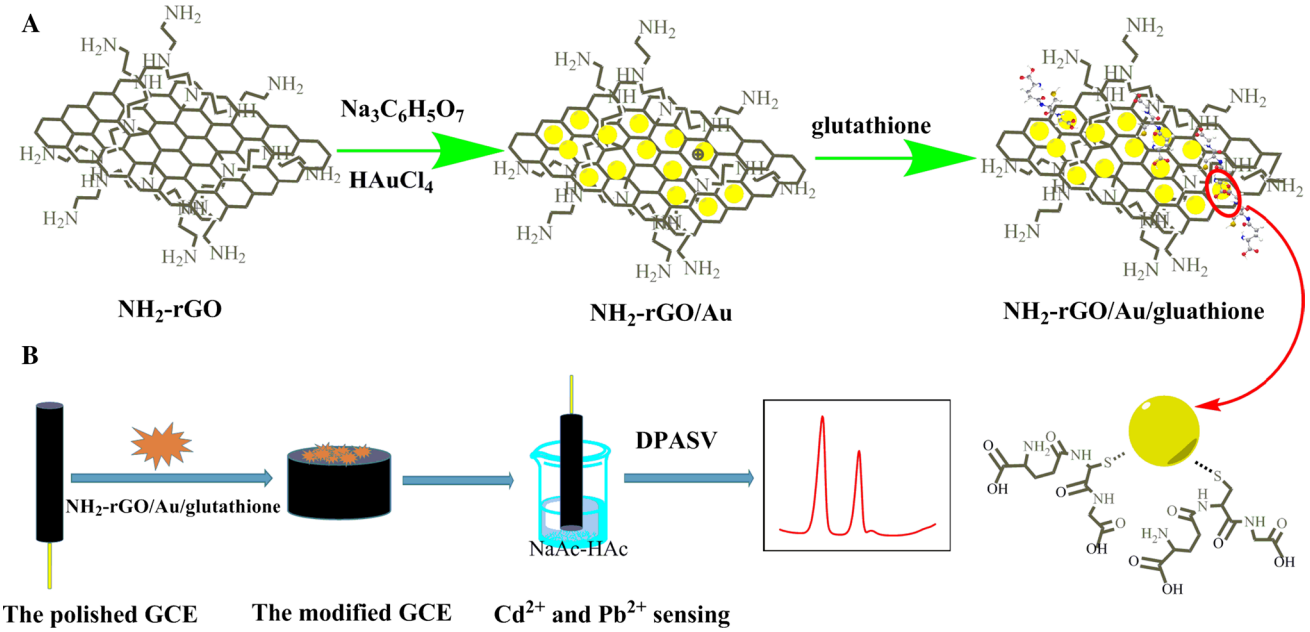

Scheme 1 Schematic diagram for the synthesis of GSH/AuNPs/NH_2-rGO (**a**) and detection process of Cd^{2+} and Pb^{2+} (**b**)

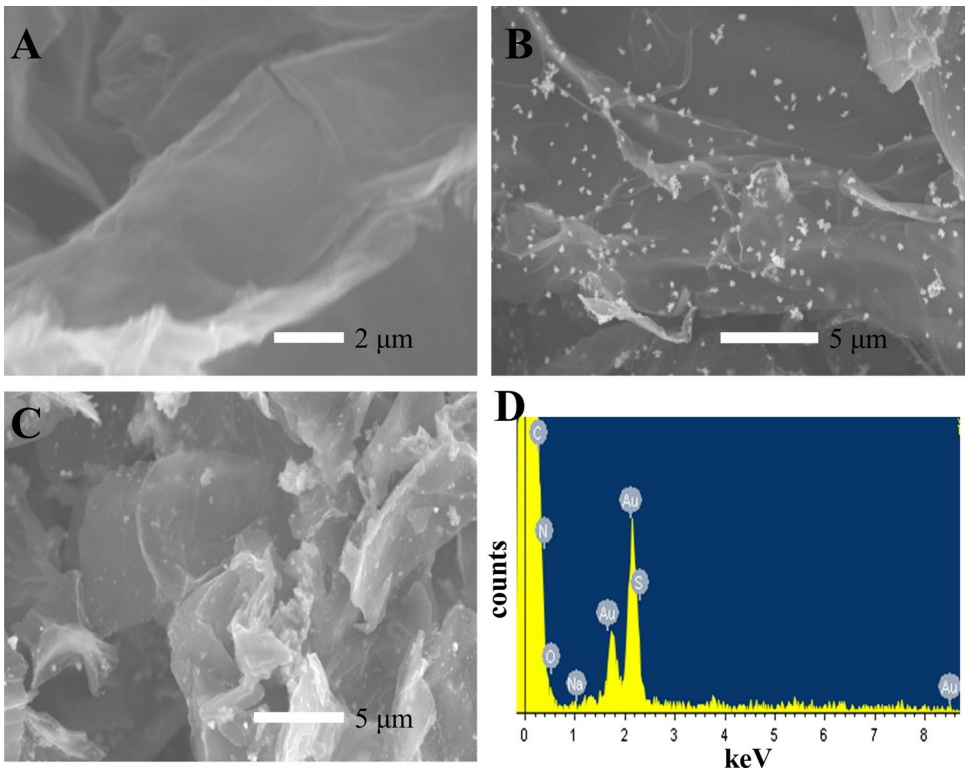

Fig. 1 **a–c** SEM images of NH_2-rGO, AuNPs/NH_2-rGO and GSH/AuNPs/NH_2-rGO, **d** EDS spectrum of GSH/AuNPs/NH_2-rGO

Whereas, the morphology of GSH/AuNPs/NH2-rGO exhibited a series of folded fragment that further increased surface area, and the especial structure was beneficial to enhancing absorbability for target metal ions (Fig. 1c). In addition, EDS analysis was performed to affirm the presence of C, N, O, S and Au (Fig. 1d), indicating the successful synthesis of GSH/AuNPs/NH_2-rGO composite.

The FTIR spectra of NH_2-rGO, AuNPs/NH_2-rGO and GSH/AuNPs/NH_2-rGO are presented in Fig. 2. For NH_2-rGO (Fig. 2a), the absorption bands at ~ 1180 cm^{-1}

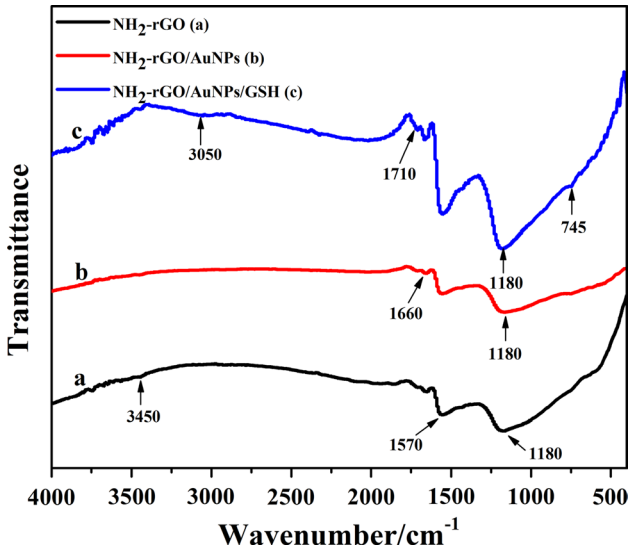

Fig. 2 FTIR spectra of NH_2-rGO (**a**), AuNPs/NH_2-rGO (**b**), GSH/AuNPs/NH_2-rGO (**c**)

and 1570 cm^{-1} were attributed to the stretching vibration of C–N and C=C, respectively (Zhou et al. 2013; Liu et al. 2017). Further, the appearance of the band at 3450 cm^{-1} was owed to the N–H bending of NH_2-rGO. The characteristic peak of NH_2-rGO/AuNPs (Fig. 2b) at ~ 1660 cm^{-1} was attributed to the vibration of $–COO^-$, indicating that citrate was attached to the AuNPs due to the synthesis process of AuNPs/NH_2-rGO (Zhu et al. 2014). The FTIR spectrum of GSH/AuNPs/NH_2-rGO (Fig. 2c) exhibited the typical absorption peaks from functional groups containing oxygen. To be specific, the bending peak at 745 cm^{-1} and absorption band at 3050 cm^{-1} can be attributed to the bending vibration and stretching vibration of –OH, respectively (Guo et al. 2017). The peak at 1710 cm^{-1} pertained to the C=O stretching vibration of COOH groups (Liu et al. 2017; Dong et al. 2015), which suggested that GSH/AuNPs/NH_2-rGO nanocomposite was successfully synthesized. Moreover, the characteristic peak of GSH at ~ 2550 cm^{-1} was not observed indicating that GSH was decorated on the surface of AuNPs through the bond of S–Au (Liu et al. 2017).

XPS analysis was employed to learn of the chemical state of the elements that were present on the GSH/AuNPs/NH_2-rGO. Figure 3a showed the survey spectrum of GSH/AuNPs/NH_2-rGO nanocomposite. The high-resolution C1s spectrum (Fig. 3b) showed four characteristic peaks at 284.5 (C–C), 285.4 (C–N), 286.3 (C–O) and 288.4 eV (C=O). The O1s core line was composed of three components (Fig. 3c). The peaks at 531.0 and 531.9 eV were assigned to the C=O and C–O, respectively. The peak at 533.2 eV corresponded to O–H bond. Moreover, the individual peak was present at 400.1 eV in N1s (Fig. 3d) spectrum corresponding to the NH. The peaks at 84.0 and 87.7 eV were attributed to $4f_{7/2}$ and $4f_{5/2}$ of Au^0, and peaks at 84.8 and 88.5 eV were ascribed to $4f_{7/2}$ and $4f_{5/2}$ of Au^+ (Fig. 3e), which indicated that the GSH/AuNPs/NH_2-rGO nanocomposite was successfully synthesized and confirmed the formation of S–Au bonds (Liu et al. 2014). The XPS spectra in the S 2p region showed peaks at 163.9 and 165.0 eV (Fig. 3f), corresponding to the S $2p_{3/2}$ and S $2p_{1/2}$ of free thiol (S–H), indicating that the GSH was decorated on the AuNPs/NH_2-rGO. Moreover, the peak at 162.0 and 163.1 eV was assigned to S–Au bonds (Minati et al. 2010; Liu et al. 2014).

Electrochemical properties of the prepared electrode

Cyclic voltammogram was an effective method to realize the surface and conductivity for the modified electrode (Xu et al. 2014; Zhou et al. 2016). The cyclic voltammetry curves of bare GCE, NH_2-rGO/GCE, AuNPs/NH_2-rGO/GCE and GSH/AuNPs/NH_2-rGO/GCE were investigated in 5 mM $[Fe(CN)_6]^{3-/4-}$ and 0.1 M KCl mixture solution with a scan rate of 100 mV/s. As shown in Fig. 4, compared with the bare GCE (a), the redox peak current of GCE modified with NH_2-rGO (b) explicitly increased ascribing to excellent electrical conductivity and vast active sites of NH_2-rGO. Moreover, the redox peak current at AuNPs/NH_2-rGO composite decorated on the electrode (c) was prominently larger than that at NH_2-rGO-modified electrode, indicating that AuNPs were distributed on NH_2-rGO and further improved the conductivity of AuNPs/NH_2-rGO composite. However, the redox peak current at GSH/AuNPs/NH_2-rGO composite-modified electrode (d) slightly decreased, which was most likely indicated that GSH hindered the electron transfer and interdicted the diffusion of $[Fe(CN)_6]^{3-/4-}$.

According to the Randles–Sevcik equation, $i_{pa} = 2.69 \times 10^5 n^{3/2} A C_0 D^{1/2} v^{1/2}$, the effective surface area can be calculated (Guo et al. 2017; Lee et al. 2016). For the equation, i_{pa} was the anodic peak current, D was the diffusion coefficient, C_0 was concentration, A was the effective surface area, v was the potential scan rate and n was the number of electrons transferred (Lee et al. 2016). All measurements were implemented with incremental scan rates using the GSH/AuNPs/NH_2-rGO/GCE and bare GCE in 5 mM $[Fe(CN)_6]^{3-/4-}$ and 0.1 M KCl mixture solution (Fig. 5a, c). As shown in Fig. 5b, d, both the redox peak currents of the modified electrode and bare electrode were in a linear correlation with the square root of scan rates at the scope of 20–200 mV/s. The effective surface area of GSH/AuNPs/NH_2-rGO/GCE was 0.089 cm^2 via calculation,

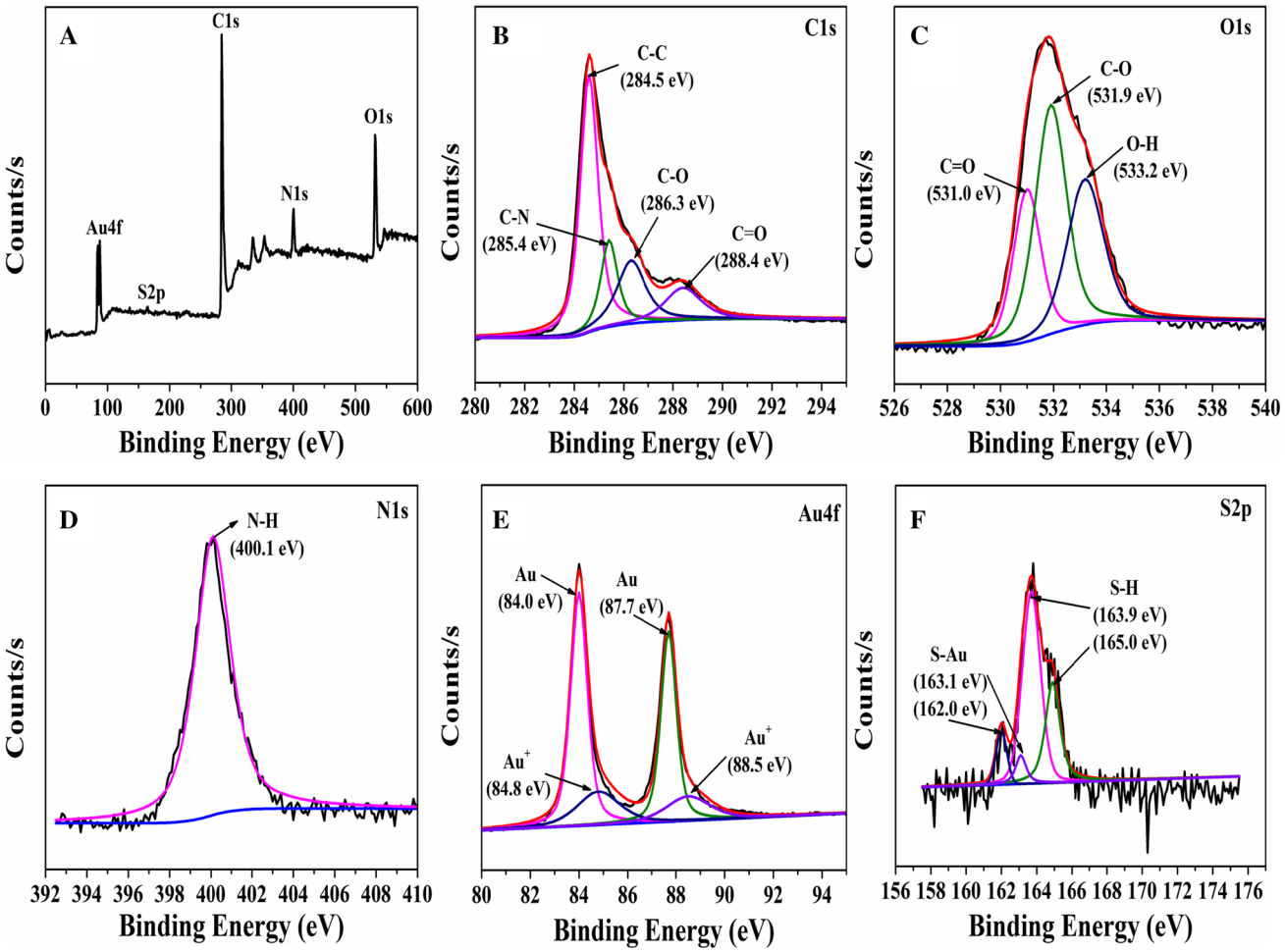

Fig. 3 XPS spectra in **a** survey, **b** C 1s region, **c** O 1s region, **d** N 1s region, **e** Au 4f region, **f** S 2p region for GSH/AuNPs/NH_2-rGO nanohybrid

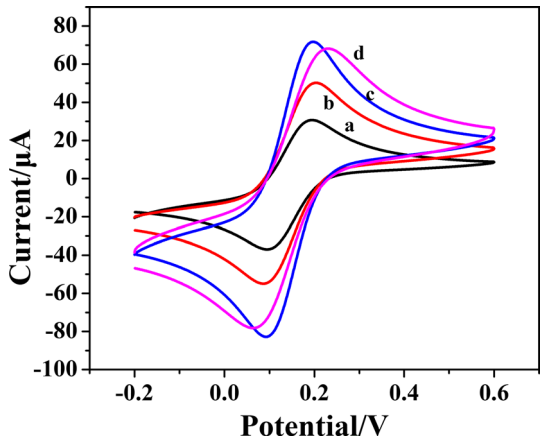

Fig. 4 Cyclic voltammograms of bare GCE (**a**), NH_2-rGO/GCE (**b**), AuNPs/NH_2-rGO/GCE (**c**) and GSH/AuNPs/NH_2-rGO/GCE (**d**)

which was 2.2 times the effective surface area of bare GCE (0.040 cm^2), indicating that GSH/AuNPs/NH_2-rGO/GCE had a larger electrochemical active area to absorb heavy metal ions.

Electrochemical signals of Cd^{2+} and Pb^{2+} at different electrodes

The stripping currents of Cd^{2+} and Pb^{2+} at different modified electrodes were studied by DPASV. The reaction happened on the electrode surface is illustrated in Scheme 2. In the deposition process, the target metal ions were adsorbed on the surface of modified nanomaterials and then reduced on the electrode surface. After the accumulation process, Cd and Pb were stripped out in the oxidation process. The more target metal ions were adsorbed on the surface of

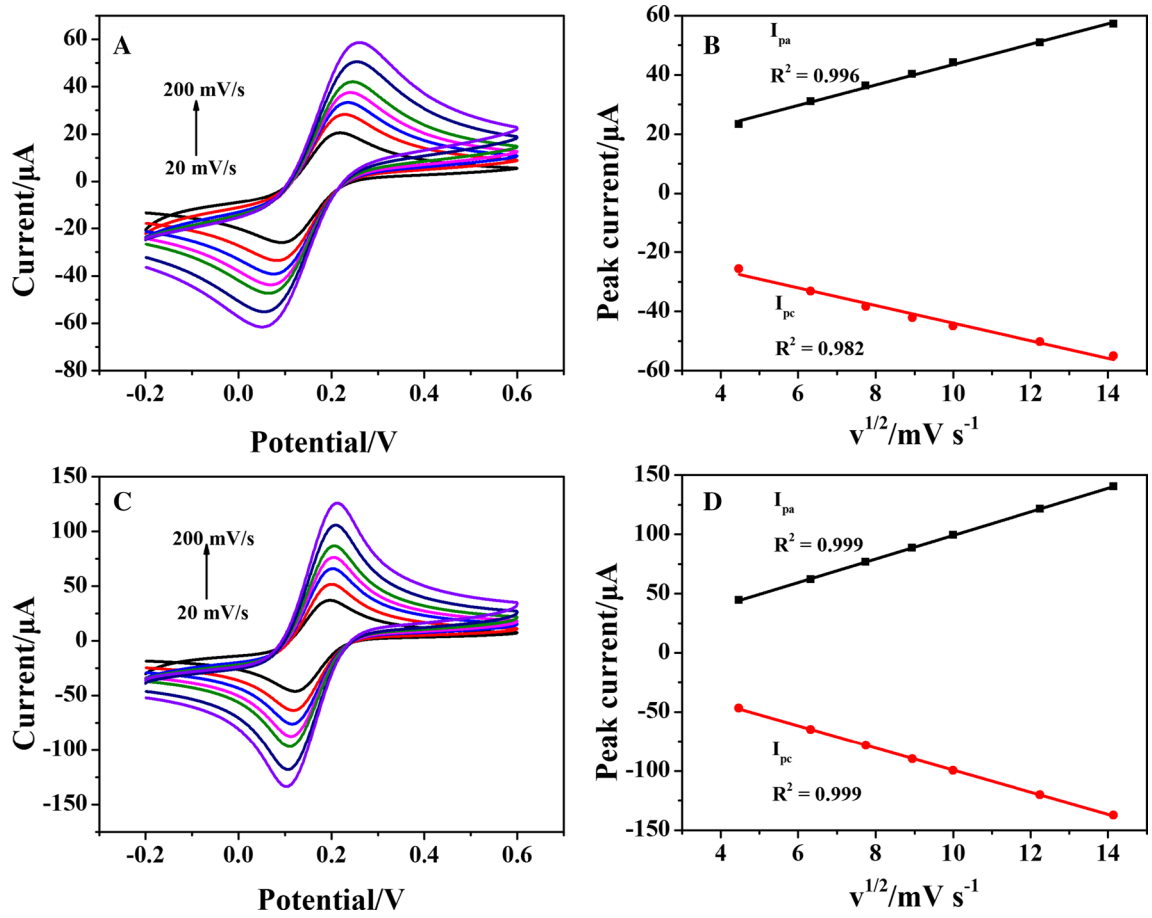

Fig. 5 Cyclic voltammograms of the bare GCE (**a**) and GSH/AuNPs/NH_2-rGO composite-modified electrode (**c**) with incremental scan rates. Plots of i_{pa}, i_{pc} vs. $v^{1/2}$ for the bare GCE (**b**) and GSH/AuNPs/NH_2-rGO composite-modified electrode (**d**)

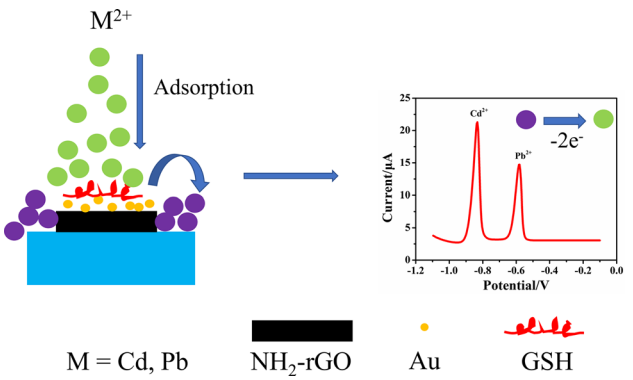

Scheme 2 Schematic diagram of Bi/GSH/AuNPs/NH_2-rGO for the electrochemical detection of heavy metal ions

nanomaterials, the larger the peak current was stripped. Figure 6 showed the analytical characteristics of bare GCE, NH_2-rGO/GCE, AuNPs/NH_2-rGO/GCE, GSH/AuNPs/NH_2-rGO/GCE and GSH/AuNPs/NH_2-rGO/GCE with a bismuth-film electrode. The DPASV was implemented in

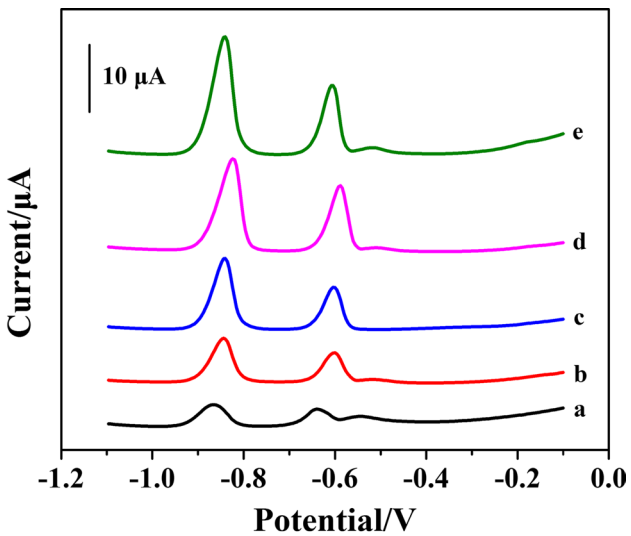

Fig. 6 DPASV responses of 25 μg/L Cd^{2+} and 25 μg/L Pb^{2+} with a deposition time of 240 s on the bare GCE (**a**), NH_2-rGO/GCE (**b**), AuNPs/NH_2-rGO/GCE (**c**), GSH/AuNPs/NH_2-rGO/GCE (**d**) and Bi/GSH/AuNPs/NH_2-rGO/GCE (**e**)

0.1 M HAc–NaAc buffer solution containing 25 μg/L Cd^{2+}, 25 μg/L Pb^{2+} and 100 μg/L Bi^{3+}.

Figure 6 (curve a) showed that the stripping peak currents of bare GCE were very weak. In contrast, the stripping peak currents of NH_2-rGO/GCE were distinctly larger than those of bare GCE, which was ascribed to the excellent electrical conductivity and plentiful amino groups of NH_2-rGO. Obviously, the AuNPs/NH_2-rGO/GCE exhibited higher signal response than NH_2-rGO/GCE because AuNPs had a higher electric conductivity and the citrate with negative charge around AuNPs had attraction effect to metal cations. Compared with AuNPs/NH_2-rGO/GCE, a remarkable rise of GSH/AuNPs/NH_2-rGO/GCE can be seen because GSH provided abundant attached ligands like –COOH groups, –SH groups, –OH groups and nitrogen functional groups. The stripping peak currents for detecting metal ions at the Bi/GSH/AuNPs/NH_2-rGO/GCE were further increased after the addition of 100 μg/L Bi^{3+} into the solution. The Bi/GSH/AuNPs/NH_2-rGO/GCE took 28.9% and 18.7% peak height enhancements for Cd^{2+} and Pb^{2+} than those of GSH/AuNPs/NH_2-rGO/GCE, indicating that Bi^{3+} can prominently enhance the preconcentration effect in the deposition process (Cao et al. 2008; Hwang et al. 2008). As a result, the Bi/GSH/AuNPs/NH_2-rGO was a promising material to detect Cd^{2+} and Pb^{2+}.

Condition optimization of the DPASV analysis

To improve the electrochemical responses to Cd^{2+} and Pb^{2+} by DPASV at Bi/GSH/AuNPs/NH_2-rGO/GCE, multifarious experimental parameters that could influence electrochemical responses were optimized.

Optimization of Bi^{3+} concentration

Figure 7a showed the effect of Bi^{3+} concentrations in the scope of 0–300 μg/L. Ranging from 0 to 200 μg/L, the stripping peak currents gradually increased, which was ascribed to the formation of a "fused alloy" with Cd^{2+} and Pb^{2+} during the deposition step (Lee et al. 2016; Hwang et al. 2008). When the Bi^{3+} concentration exceeded 200 μg/L, the stripping peak currents of Cd^{2+} and Pb^{2+} simultaneously declined. Therefore, the optimal Bi^{3+} concentration was determined to be 200 μg/L.

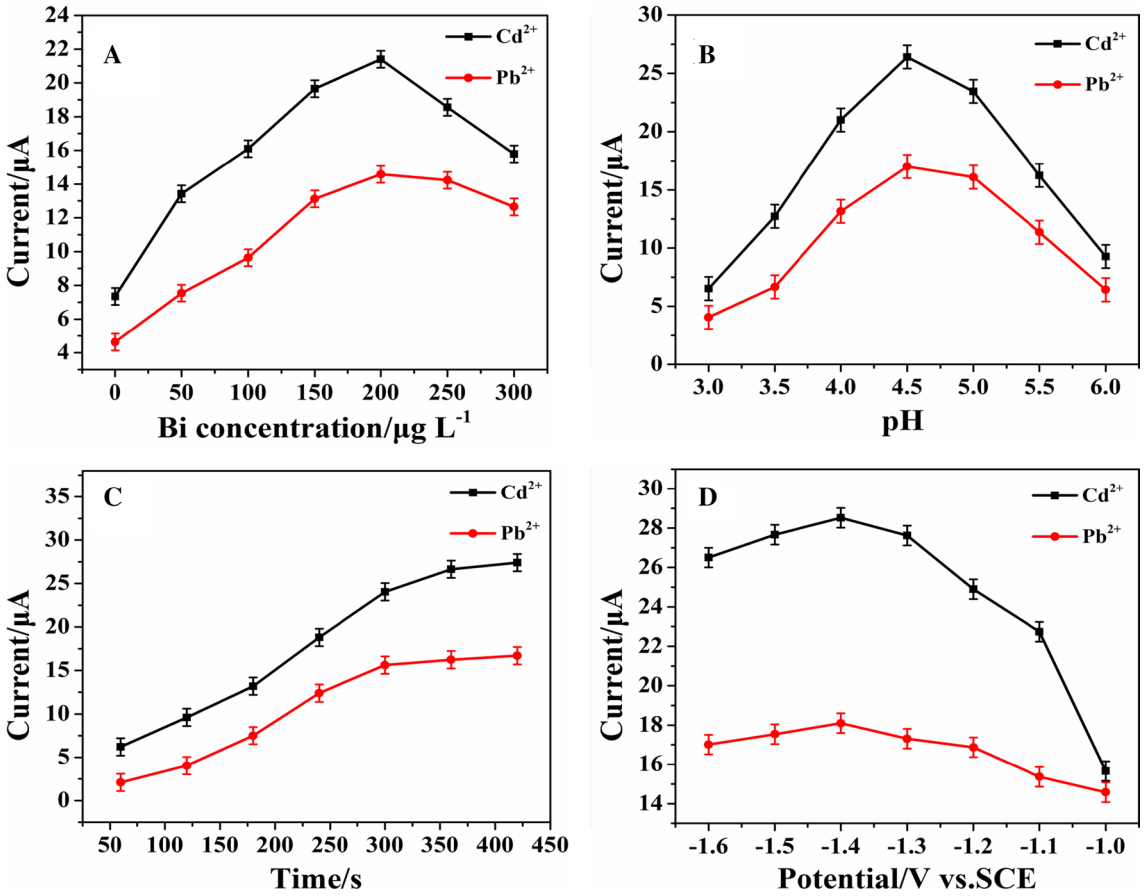

Fig. 7 The effect of Bi^{3+} concentration (**a**), pH value (**b**), preconcentration time (**c**) and deposition potential (**d**) on the stripping peak current at Bi/GSH/AuNPs/NH_2-rGO/GCE in 0.1 M acetate buffer solution (pH 4) containing 25 μg/L Cd^{2+} and 25 μg/L Pb^{2+}

Optimization of pH value

As shown in Fig. 7b, both stripping peak currents enhanced with pH value at a scope from 3.0 to 4.5. It can be explained as follows: at the low pH range, protons could bind to hydrophilic groups of the NH_2-rGO and GSH, leading to the reduction of target ions at the preconcentration step. Whereas, the response currents of target metal ions declined when pH value exceeded 4.5, indicating that hydroxide precipitate was formed due to the hydrolysis of target metal ions. Therefore, pH 4.5 was regarded as the optimal pH value.

Optimization of preconcentration time

The influence of preconcentration time in the scope of 60–420 s on electrochemical responses was investigated by DPASV. Figure 7c showed that the response currents of Cd^{2+} and Pb^{2+} increased rapidly in the range of 60–300 s. However, the response currents of Cd^{2+} and Pb^{2+} rose slightly after the preconcentration time exceeded 300 s, so 300 s was selected as optimization value given the sensitivity and efficiency.

Optimization of deposition potential

In the accumulation and stripping process, the usage of appropriate deposition potential was crucial for improving sensitivity. Figure 7d showed that the deposition potential affected the response currents. Specifically, the response currents exhibited a significant growth trend ranging from − 1.0 to − 1.4 V, and then gradually declined because of hydrogen evolution (Xiao et al. 2014). The maximum stripping peak current could be observed at − 1.4 V for the two heavy metals. Hence, the optimal value was determined to be − 1.4 V for subsequent measurements.

Analytical performance for the simultaneous detection of Cd^{2+} and Pb^{2+}

The DPASV responses for Cd^{2+} and Pb^{2+} on Bi/GSH/AuNPs/NH_2-rGO/GCE were performed with incremental metal ion

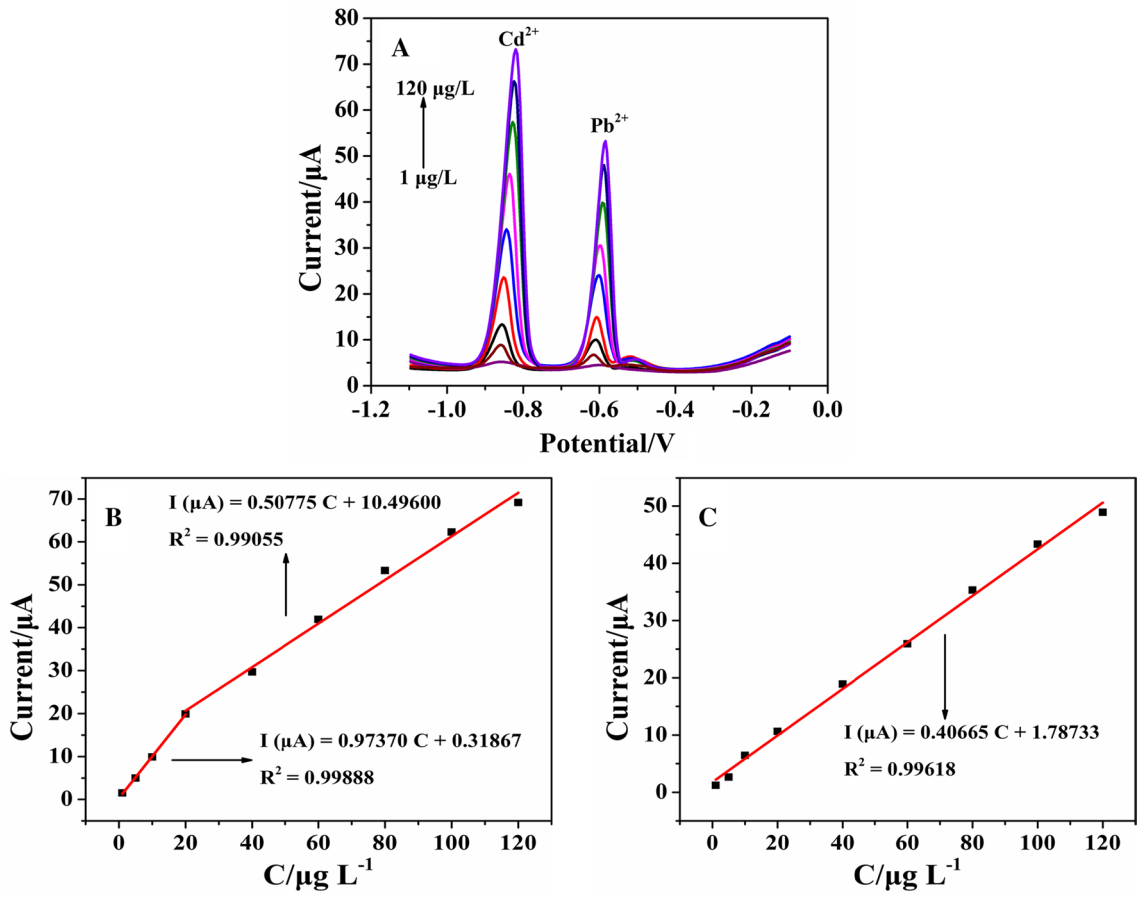

Fig. 8 **a** Current responses of the Bi/GSH/AuNPs/NH_2-rGO/GCE for simultaneous detection of different Cd^{2+} and Pb^{2+} concentrations; the linear relationship between the response currents and incremental concentration of Cd^{2+} (**b**) and Pb^{2+} (**c**)

Table 1 Comparison of the analytical performance of different methods

Electrode	Technique	Linear range (μg/L)		Detection limit (μg/L)		References
		Cd^{2+}	Pb^{2+}	Cd^{2+}	Pb^{2+}	
Nafion/Bi/NMC/GCE	DPASV	2–100	0.5–100	1.5	0.05	Xiao et al. (2014)
Bi/Au-GN-Cys/GCE	SWASV	0.50–40	0.50–40	0.10	0.05	Zhu et al. (2014)
L-cys/GR-CS/GCE	DPASV	0.56–67.2	1.04–62.1	0.45	0.12	Zhou et al. (2016)
Bi/Fe_2O_3/G/GCE	DPASV	1–100	1–100	0.08	0.07	Lee et al. (2016)
Bi/MWCNT-EBP-NA/GCE	SWASV	1–50	1–50	0.06	0.08	Zhao et al. (2016)
Bi/CNT/SPE	ASV	2–100	2–100	0.7	1.3	Hwang et al. (2008)
Nafion/G/PANI	SWASV	1–300	1–300	0.1	0.1	Ruecha et al. (2015)
Bi/GSH/AuNPs/NH_2-rGO/GCE	DPASV	1–120	1–120	0.09	0.38	This work

concentrations under the optimum experimental conditions. As shown in Fig. 8a, the sharp peak currents were enhanced with incremental Cd^{2+} and Pb^{2+} concentrations. Figure 8b exhibited that the response currents were linear with Cd^{2+} concentrations in the scope of 1–120 μg/L. The linear equations were I (μA) = 0.31867 + 0.97370 C (μg/L) (R^2 = 0.99888) and I (μA) = 10.49600 + 0.50775 C (μg/L) (R^2 = 0.99055), respectively. The detection limit was calculated to be 0.09 μg/L (S/N = 3) (Huang et al. 2015). Similarly, Fig. 8c exhibited that the response currents were linear with Pb^{2+} concentration in the scope of 1–120 μg/L. The linear equation was I (μA) = 1.78733 + 0.40665 C (μg/L) (R^2 = 0.99618) with the detection limit of 0.38 μg/L. The detection performance of Cd^{2+} and Pb^{2+} in the propositional method was compared with other methods which have been reported before and the electrode was modified with carbon-based materials. The results are summarized in Table 1. It was clear that the linear range in this work was wider than most of the developed methods, which meant it had an extensive concentration range to detect Cd^{2+} and Pb^{2+}. Moreover, it can be noticed that the detection limit of Cd^{2+} and Pb^{2+} was at an average level compared with most of those methods. As mentioned above, it was obvious that the propositional sensor had superior performance ascribing to the synergistic effect of NH_2-rGO, AuNPs, GSH and the bismuth film on the deposition of Cd^{2+} and Pb^{2+}.

Reproducibility, stability, and interference of Bi/GSH/AuNPs/NH_2-rGO/GCE

The reproducibility and stability were demonstrated with the same Bi/GSH/AuNPs/NH_2-rGO/GCE which was stored in the air over 2 weeks. After the experimental parameters were optimized, the prepared electrode was tested for 10 times in 0.1 M HAc–NaAc buffer solution containing 15 μg/L Cd^{2+} and 15 μg/L Pb^{2+}. As shown in Fig. 9, the RSD were 1.48% and 3.34% for Cd^{2+} and Pb^{2+}, respectively. It revealed that the Bi/GSH/AuNPs/NH_2-rGO/GCE had good reproducibility and long-term stability.

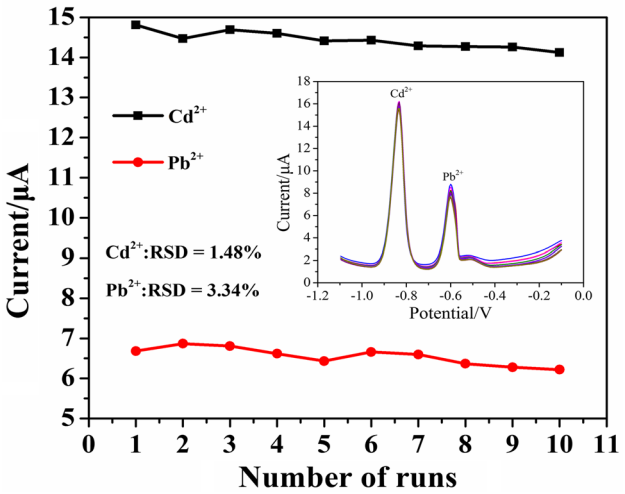

Fig. 9 Stripping current measurements of 15 μg/L Cd^{2+} and 15 μg/L Pb^{2+} on the Bi/GSH/AuNPs/NH_2-rGO/GCE. The illustration corresponds to current responses for 10 times

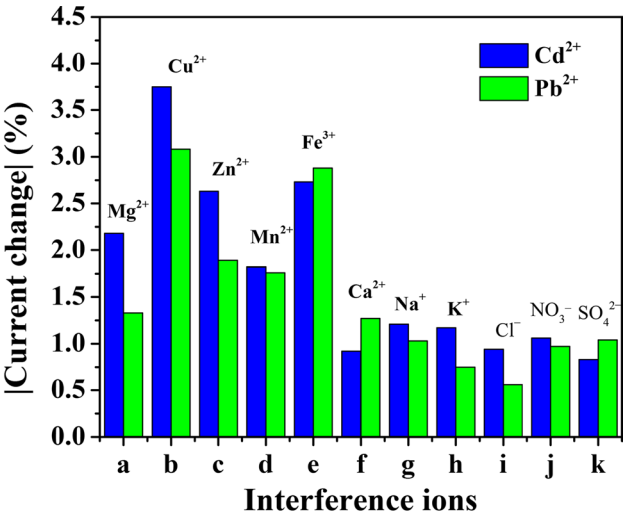

Fig. 10 The stripping peak current changes of Cd^{2+} and Pb^{2+} with interfering ions are listed in order (**a**–**k**): **a** Mg^{2+}, **b** Cu^{2+}, **c** Zn^{2+}, **d** Mn^{2+}, **e** Fe^{3+}, **f** Ca^{2+}, **g** Na^{+}, **h** K^{+}, **i** Cl^{-}, **j** NO_3^{-}, **k** SO_4^{2-}

Table 2 Recovery result for Cd^{2+} and Pb^{2+} in tap water

Heavy metal ions	Added (μg/L)	Found (μg/L)	Recovery (%)
Cd^{2+}	5	4.91	98.20
	15	14.39	95.73
	50	49.16	98.32
Pb^{2+}	5	4.78	95.60
	15	14.56	97.06
	50	49.42	98.84

In addition, the anti-interference ability was tested in the presence of 20-fold Mg^{2+}, Cu^{2+}, Zn^{2+}, Mn^{2+}, Fe^{3+}, Ca^{2+}, Na^{+}, K^{+}, Cl^{-}, NO_3^{-} and SO_4^{2-}. The result is shown in Fig. 10. It can be noticed that the changes of both stripping peak currents were within 4% for Cd^{2+} and Pb^{2+}, which proved that the Bi/GSH/AuNPs/NH_2-rGO/GCE had excellent selectivity for target metal ions.

Application of real samples

To evaluate its feasibility in real samples, the proposed electrode was exploited to detect Cd^{2+} and Pb^{2+} in tap water through the standard addition method. The result is summarized in Table 2. The recovery of Cd^{2+} was 95.73–98.32%, and the recovery of Pb^{2+} was 95.60–98.84%, indicating that Bi/GSH/AuNPs/NH_2-rGO/GCE can be applied as an effective and precise method to determine Cd^{2+} and Pb^{2+}.

Conclusions

An original method for the simultaneous detection of Cd^{2+} and Pb^{2+} based on Bi/GSH/AuNPs/NH_2-rGO-modified GCE was developed. Owing to the synergistic effect of composite materials, such as strong electron transfer ability, large effective surface area and strong adsorption capability, the prepared Bi/GSH/AuNPs/NH_2-rGO/GCE exhibited excellent electrochemical properties. This working electrode was employed to simultaneously detect Cd^{2+} and Pb^{2+}, and it showed a good linear proportionality from 1 to 120 μg/L with low detection limits of 0.09 μg/L and 0.38 μg/L, respectively, which were well below standard in potable water given by WHO (Cd^{2+} is below 3 μg/L and Pb^{2+} is below 10 μg/L), suggesting that the electrode can be applied to potable water monitoring of Cd^{2+} and Pb^{2+}. Moreover, the proposed method was successfully exploited for the analysis of the tap water samples.

Acknowledgements This work was supported by the Natural Science Foundations of Zhejiang Province [Grant No. LY17F010021].

Compliance with ethical standards

Conflict of interest On behalf of all authors, the corresponding author states that there is no conflict of interest.

References

Bagheri H, Afkhami A, Sabertehrani M, Khoshsafar H (2012) Preparation and characterization of magnetic nanocomposite of Schiff base/silica/magnetite as a preconcentration phase for the trace determination of heavy metal ions in water, food and biological samples using atomic absorption spectrometry. Talanta 97:87–95. https://doi.org/10.1016/j.talanta.2012.03.066

Cao L, Jia J, Wang Z (2008) Sensitive determination of Cd and Pb by differential pulse stripping voltammetry with in sit-u bismuth-modified zeolite doped carbon paste electrodes. Electrochim Acta 53(5):2177–2182. https://doi.org/10.1016/j.electacta.2007.09.024

Cheng YM, Fa HB, Yin W et al (2016) A sensitive electrochemical sensor for lead based on gold nanoparticles/nitrogen-doped graphene composites functionalized with L-cysteine-modified electrode. J Solid State Electrochem 20(2):327–335. https://doi.org/10.1007/s10008-015-3043-0

Choi SM, Kim DM, Jung OS, Shim YB (2015) A disposable chronocoulometric sensor for heavy metal ions using a diam-inoterthiophene-modified electrode doped with graphene oxide. Anal Chim Acta 892:77–84. https://doi.org/10.1016/j.aca.2015.08.037

Dong Z, Zhang F, Wang D et al (2015) Polydopamine-mediated surface-functionalization of graphene oxide for heavy metal ions removal. J Solid State Chem 224:88–93. https://doi.org/10.1016/j.jssc.2014.06.030

Guo Z, Li DD, Luo XK et al (2017) Simultaneous determination of trace Cd(II), Pb(II) and Cu(II) by differential pulse anodic stripping voltammetry using a reduced graphene oxide-chitosan/poly-L-lysine nanocomposite modified glassy carbon electrode. J Colloid Interface Sci 490:11–22. https://doi.org/10.1016/j.jcis.2016.11.006

Gupta VK, Yola ML, Atar N, Ustundag Z, Solak AO (2013) A novel sensitive Cu(II) and Cd(II) nanosensor platform gra-phene oxide terminated p-aminophenyl modified glassy carbon surface. Electrochim Acta 112:541–548. https://doi.org/10.1016/j.electacta.2013.09.011

Guzmánmar JL, Hinojosa-Reyes L, Serra AM, Hernández-Ramírez A, Cerdà V (2011) Applicability of multisyringe chromatography coupled to cold-vaporatomic fluorescence spectrometry for mercury speciation analysis. Anal Chim Acta 708(1):11–18. https://doi.org/10.1016/j.aca.2011.09.037

Han L, Liu CM, Dong SL, Du CX, Zhang XY, Li LH, Wei Y (2017) Enhanced conductivity of rGO/AgNPs composites f-or electrochemical immunoassay of prostate-specific antigen. Biosens Bioelectron 87:466–472. https://doi.org/10.1016/j.bios.2016.08.004

Ho TY, Chien CT, Wang BN et al (2010) Determination of trace metals in seawater by an automated flow injection ion chromatograph pretreatment system with ICPMS. Talanta 82(4):0–1484. https://doi.org/10.1016/j.talanta.2010.07.022

Huang S, Lu SY, Huang CS et al (2015) Sensitive and selective stripping voltammetric determination of copper(II) using a glassy carbon electrode modified with amino-reduced graphene oxide and

β-cyclodextrin. Microchim Acta 182(15–16):2529–2539. https://doi.org/10.1007/s00604-015-1627-0

Hwang GH, Han WK, Park JS et al (2008) Determination of trace metals by anodic stripping voltammetry using a bismuth-modified carbon nanotube electrode. Talanta 76(2):301–308. https://doi.org/10.1016/j.talanta.2008.09.028

Injang U, Noyrod P, Siangproh W et al (2010) Determination of trace heavy metals in herbs by sequential injection analysis anodic stripping voltammetry using screen-printed carbon nanotubes electrodes. Anal Chim Acta 668(1):54–60. https://doi.org/10.1016/j.aca.2010.01.018

Lee S, Oh J, Kim D et al (2016) A sensitive electrochemical sensor using an iron oxide/graphene composite for the simultaneous detection of heavy metal ions. Talanta 160:528–536. https://doi.org/10.1016/j.talanta.2016.07.034

Liu WJ, Sun DR, Fu JL et al (2014) Assembly of evenly distributed Au nanoparticles on thiolated reduced graphene oxide as an active and robust catalyst for hydrogenation of 4-nitroarenes. RSC Adv 4:11003–11011. https://doi.org/10.1039/c3ra47829g.2014.04.021

Liu FM, Zhang Y, Yin W et al (2017) A high–selectivity electrochemical sensor for ultra-trace lead (II) detection based on a nanocomposite consisting of nitrogen-doped graphene/gold nanoparticles functionalized with ETBD and Fe_3O_4@TiO_2 core-shell nanoparticles. Sens Actuators B Chem 242:889–896. https://doi.org/10.1016/j.snb.2016.09.167

Ma Y, Liu H, Qian K, Yang L, Liu J (2012) A displacement principle for mercury detection by optical wave guide and surface enhanced Raman spectroscopy. J. Colloid Inter. Sci 386:451–455. https://doi.org/10.1016/j.jcis.2012.07.067

Minati L, Speranza G, Torrengo S et al (2010) Characterization of thiol-functionalized carbon nanotubes on gold surfaces. Surf Sci 604(17):1414–1419. https://doi.org/10.1016/j.susc.2010.05.002

Ruecha N, Rodthongkum N, Cate DM et al (2015) Sensitive electrochemical sensor using a graphene-polyaniline nanocom-posite for simultaneous detection of Zn(II), Cd(II), and Pb(II). Anal Chim Acta 874:40–48. https://doi.org/10.1016/j.aca.2015.02.064

Wang X, Falk M, Ortiz R, Matsumura H, Bobacka J et al (2012) Mediatorless sugar/oxygen enzymatic fuel cells based on gold nanoparticle-modified electrodes. Biosens Bioelectron 31:219–225. https://doi.org/10.1016/j.bios.2011.10.020

Xiao L, Xu H, Zhou S et al (2014) Simultaneous detection of Cd(II) and Pb(II) by differential pulse anodic stripping vol-tammetry at a nitrogen-doped microporous carbon/Nafion/bismuth-film electrode. Electrochim Acta 143:143–151. https://doi.org/10.1016/j.electacta.2014.08.021

Xie YL, Zhao SQ, Ye HL, Yuan J, Song P, Hu SQ (2015) Graphene/CeO_2 hybrid materials for the simultaneous electroc-hemical detection of cadmium(II), lead(II), copper(II), and mercury(II). J Electroanal Chem 757:235–242. https://doi.org/10.1016/j.jelechem.2015.09.043

Xing H, Xu J, Zhu X et al (2016) A new electrochemical sensor based on carboimidazole grafted reduced graphene oxidefor simultaneous detection of Hg^{2+}, and Pb^{2+}. J Electroanal Chem 782:250–255. https://doi.org/10.1016/j.jelechem.2016.10.043

Xu XX, Duan GT, Li Y et al (2014) Fabrication of gold nanoparticles by laser ablation in liquid and their application fo-r simultaneous electrochemical detection of Cd^{2+}, Pb^{2+}, Cu^{2+}, Hg^{2+}. ACS Appl Mater Interfaces 6(1):65–71. https://doi.org/10.1021/am404816e

Zhao G, Yin Y, Wang H et al (2016) Sensitive stripping voltammetric determination of Cd(II) and Pb(II) by a Bi/multi-walled carbon nanotube-emeraldine base polyaniline-Nafion composite modified glassy carbon electrode. Electrochim Acta 220:267–275. https://doi.org/10.1016/j.electacta.2016.10.059

Zhou Y, Hu X, Zhang M et al (2013) Preparation and characterization of modified cellulose for adsorption of Cd(II), H-g(II), and acid fuchsin from aqueous solutions. Ind Eng Chem Res 52(2):876–884. https://doi.org/10.1021/ie301742h

Zhou WS, Li CH, Sun C et al (2016) Simultaneously determination of trace Cd^{2+} and Pb^{2+} based on L-cysteine/graphene modified glassy carbon electrode. Food Chem 192:351–357. https://doi.org/10.1016/j.foodchem.2015.07.042

Zhu L, Xu L, Huang B et al (2014) Simultaneous determination of Cd(II) and Pb(II) using square wave anodic stripping voltammetry at a gold nanoparticle-graphene-cysteine composite modified bismuth film electrode. Electrochim Acta 115:471–477. https://doi.org/10.1016/j.electacta.2013.10.209